EINDHOVEN UNIVERSITY OF TECHNOLOGY

Theory of superfast fronts of impact ionization in semiconductor structures

Citation for published version (APA):
Rodin, P., Ebert, U., Minarsky, A., & Grekhov, I. V. (2007). Theory of superfast fronts of impact ionization in semiconductor structures. *Journal of Applied Physics*, *102*(3), 034508-1/13. Article 034508. https://doi.org/10.1063/1.2767378

DOI:
10.1063/1.2767378

Document status and date:
Published: 01/01/2007

Document Version:
Publisher’s PDF, also known as Version of Record (includes final page, issue and volume numbers)

Please check the document version of this publication:

• A submitted manuscript is the version of the article upon submission and before peer-review. There can be important differences between the submitted version and the official published version of record. People interested in the research are advised to contact the author for the final version of the publication, or visit the DOI to the publisher's website.
• The final author version and the galley proof are versions of the publication after peer review.
• The final published version features the final layout of the paper including the volume, issue and page numbers.

Link to publication

General rights
Copyright and moral rights for the publications made accessible in the public portal are retained by the authors and/or other copyright owners and it is a condition of accessing publications that users recognise and abide by the legal requirements associated with these rights.

• Users may download and print one copy of any publication from the public portal for the purpose of private study or research.
• You may not further distribute the material or use it for any profit-making activity or commercial gain
• You may freely distribute the URL identifying the publication in the public portal.

If the publication is distributed under the terms of Article 25fa of the Dutch Copyright Act, indicated by the “Taverne” license above, please follow below link for the End User Agreement:

www.tue.nl/taverne

Take down policy
If you believe that this document breaches copyright please contact us at:

openaccess@tue.nl

providing details and we will investigate your claim.

Download date: 16. Nov. 2023

JOURNAL OF APPLIED PHYSICS 102, 034508 (2007)

Theory of superfast fronts of impact ionization in semiconductor structures

Pavel Rodin[a)]
Ioffe Physicotechnical Institute of Russian Academy of Sciences, Politechnicheskaya 26, 194021, St. Petersburg, Russia

Ute Ebert
Centrum voor Wiskunde en Informatica, Postbus 94079, 1090 GB Amsterdam, The Netherlands

Andrey Minarsky
Physico-Technical High School of Russian Academy of Sciences, Khlopina 8-3,194021, St. Petersburg, Russia

Igor Grekhov
Ioffe Physicotechnical Institute, Politechnicheskaya 26, 194021, St. Petersburg, Russia

(Received 29 April 2007; accepted 22 June 2007; published online 9 August 2007)

We present an analytical theory for impact ionization fronts in reversely biased p^+-n-n^+ structures. The front propagates into a depleted n base with a velocity that exceeds the saturated drift velocity. The front passage generates a dense electron-hole plasma and in this way switches the structure from low to high conductivity. For a planar front we determine the concentration of the generated plasma, the maximum electric field, the front width, and the voltage over the n base as functions of front velocity and doping of the n base. The theory takes into account that drift velocities and impact ionization coefficients differ between electrons and holes, and it makes quantitative predictions for any semiconductor material possible. © *2007 American Institute of Physics*.
[DOI: 10.1063/1.2767378]

I. INTRODUCTION

Fronts of impact ionization can be excited in layered semiconductor structures such as p^+-n-n^+ diodes and p^+-n-p-n^+ dynistors.[1–9] The front passage fills the structure with dense electron-hole plasma and hence leads to the transition of the reversely biased p-n junction from low-conducting to high conducting state. Apart from microwave TRAPATT (TRApped Plasma Avalanche Triggered Transit) diodes[1,2] triggering of impact ionization fronts has been observed in high-voltage p^+-n-n^+ diodes manufactured from both Si (Refs. 3–6) and GaAs.[7–9] In modern semiconductor electronics, excitation of ionization front is a unique nonoptical method capable of forming subnanosecond voltage ramps with kilovolt amplitudes. It has found numerous pulse power applications.[10,11]

The mechanism of front propagation is based on avalanche multiplication of carriers by impact ionization and subsequent screening of the ionizing electric field due to the Maxwellian relaxation in the generated electron-hole plasma. The qualitative picture of the front passage is well-known (e.g., see Ref. 12 and references therein). In Fig. 1 we sketch the profiles of the electric field E and the total carrier concentration $\sigma=n+p$ (here n and p are concentrations of electron and hole, respectively) in the n base of reversely biased p^+-n-n^+ diode structure. The front propagates into a *depleted region* where the concentration of free carriers σ_0 is much smaller than the concentration of dopants N_d. In the depleted region the slope of electric field $qN_d/\varepsilon\varepsilon_0$ is controlled by the charge of ionized donors. The *ionization zone* travels into the depleted region with velocity v_f that exceeds the saturated drift velocity v_{ns} of electrons. This is possible due to a small concentration of free carriers σ_0 in the depleted region. The multiplication of these carriers starts as soon as the electric field becomes sufficiently strong; therefore, the ionization zone can propagate faster than the drift velocity. Generation of electron-hole pairs and subsequent separation of electron

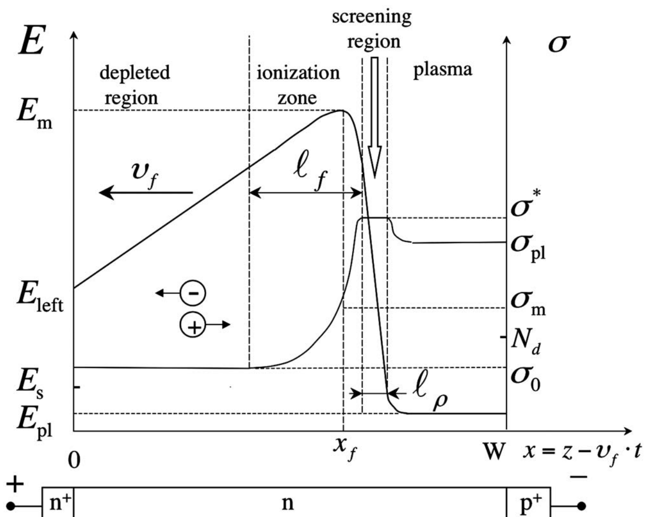

FIG. 1. Sketch of the electric field E and total concentration of free carriers concentrations $\sigma=n+p$ (lower panel) in the p^+-n-p^+ structure during the passage of the ionization front. The field E_s corresponds to the transition from linear low-field transport to saturated drift velocities. Coordinates x and $z=x+v_ft$ correspond to stationary and comoving frames, respectively. Note relations $\sigma_0 \ll N_d, \sigma^\star, \sigma_{pl}$ and between the initial concentration σ_0 in the depleted region, doping N_d and plasma concentration σ_{pl}. The relation $\sigma^\star > \sigma_{pl}$ generally holds only for $v_{ns} > v_{ps}$ and can be broken for $v_{ns} < v_{ps}$.

a)Electronic mail: rodin@mail.ioffe.ru

 © 2007 American Institute of Physics

Downloaded 11 Mar 2010 to 131.155.151.137. Redistribution subject to AIP license or copyright; see http://jap.aip.org/jap/copyright.jsp

and hole in the electric field forms a *screening region* behind the ionization zone. Here the drift velocities remain saturated. The space charge in the screening region is due to excessive electron concentration. In the *plasma* layer the carrier concentration $\sigma_{\rm pl}$ exceeds N_d by several orders of magnitude; electric field is low and corresponds to linear ohmic regime. The described propagation of ionization front resembles the propagation of fingerlike streamers into preionized medium (see the discussion in Ref. 13).

The analytical theory of traveling ionization fronts in p^+-n-n^+ structures has been pioneered in Ref. 2 for TRAPATT diodes. This classical work is based on two crucial simplifications that make the theory essentially qualitative: (i) impact ionization coefficients are modeled by step functions; and (ii) electrons and holes are assumed to be identical. Later on the focus mostly shifted from analytical studies to numerical simulations.[14–16] The demand for a quantitative analytical description remains strong, in particular, as ionization fronts in wideband materials[17] and also operation at electric fields above the band-to-band Zener breakdown[18,19] have a promising prospective. Analytical theory is also important to place ionization fronts in doped semiconductor structures into the general context of studies on front dynamics in spatially extended nonlinear systems.[20–22]

This article presents a theory of ionization front in a reversely biased p^+-n-n^+ structure. We take the asymmetry between electron and holes in both transport and impact ionization into account and assume a general form of impact ionization coefficients. The theory determines the maximum electric field in the traveling front E_m, the voltage over the structure u, the concentration of the generated plasma $\sigma_{\rm pl}$, and the electric field in plasma $E_{\rm pl}$ as functions of front velocity v_f and the n base doping N_d for self-similar propagation with constant velocity v_f. These results determine the instant front velocity v_f as a function of the applied voltage u and front position x_f in cases when the front velocity and shape vary during the passage.

II. MODEL

A. Basic equations in drift-diffusion approximation

We investigate how an impact ionization front passes through a uniformly doped n base of a reversely biased p^+-n-n^+ diode structure as sketched in Fig. 1. Heavily doped p^+ and n^+ layers play the role of contacts and are not taken into further consideration. The carrier dynamics in the n base is described by the standard set of continuity equations and the Poisson equation,

$$\partial_t n - \partial_x[v_n(E)n] - D_n\partial_x^2 n = G(n,p,E),$$

$$\partial_t p + \partial_x[v_p(E)p] - D_p\partial_x^2 p = G(n,p,E),$$

$$\partial_x E = \frac{q}{\varepsilon\varepsilon_0}(p - n + N_d), \quad (1)$$

where n,p and v_n,v_p are electron and hole concentrations and drift velocities, respectively, E is the electric field strength, N_d=constant is concentration of donors in the n base, $q>0$ is the elementary charge, ε and ε_0 are the permittivity of the material and the absolute permittivity, respectively. We use the notation $v_{n,p}(E)>0$ and take the actual direction of the carrier drift through the signs in Eqs. (1) into account. The impact ionization term is given by

$$G(n,p,E) = \alpha_n(E)v_n(E)n + \alpha_p(E)v_p(E)p, \quad (2)$$

where $\alpha_{n,p}(E)$ are impact ionization coefficients.

Let us introduce new variables,

$$\sigma \equiv n + p, \quad \rho \equiv p - n. \quad (3)$$

The first variable σ is the total concentration of free carriers, the second one ρ is proportional to the space charge of free carriers. Neglecting diffusion that does not play any role in the relevant scales (e.g., see Ref. 13), we present Eqs. (1) as

$$\partial_t\sigma + \partial_x[v^-(E)\sigma + v^+(E)\rho] = 2G, \quad (4)$$

$$\partial_t\rho + \partial_x[v^+(E)\sigma + v^-(E)\rho] = 0, \quad (5)$$

$$\partial_x E = \frac{q}{\varepsilon\varepsilon_0}[\rho + N_d], \quad (6)$$

where

$$v^+(E) \equiv \frac{v_p(E) + v_n(E)}{2}, \quad v^-(E) \equiv \frac{v_p(E) - v_n(E)}{2}. \quad (7)$$

Note that for most semiconductors $v^-(E)<0$.

Solving Eq. (6) for ρ, substituting this ρ into the expression $\partial_t\rho$ in Eq. (5), and integrating over x, we obtain the conservation of the total current density in a one-dimensional system,

$$J = q[v^+(E)\sigma + v^-(E)\rho] + \varepsilon\varepsilon_0\partial_t E,$$

$$\partial_x J = 0. \quad (8)$$

Here, the first and the second term correspond to the conduction and displacement components of the current density J, respectively. In the following we replace Eq. (5) by Eq. (8).

B. Self-similar propagation of the ionization front

We consider the fronts moving in the same direction as electrons drift—so-called *negative* fronts. We choose $E>0$; hence, electrons and negative fronts move to the left (cf. Fig. 1).

Positive fronts in n^+-p-p^+ structures that move in the same direction as hole drift can be described by exchanging electrons and holes in Eqs. (1) and replacing the donor concentration N_d by the same acceptor concentration N_a. For the self-similar front motion with velocity v_f=constant, we get

$$\sigma(x,t) = \sigma(x + v_f t),$$

$$\rho(x,t) = \rho(x + v_f t),$$

$$E(x,t) = E(x + v_f t),$$

where we fixed the notation such that the fronts move with a positive velocity $v_f>0$ in the negative x direction. Then, in the comoving frame $z \equiv x + v_f t$, Eqs. (4), (8), and (6) become

$$d_z[(v_f + v^-)\sigma + v^+\rho] = 2G, \quad (9)$$

Downloaded 11 Mar 2010 to 131.155.151.137. Redistribution subject to AIP license or copyright; see http://jap.aip.org/jap/copyright.jsp

$$J = q[v^+\sigma + v^-\rho] + \varepsilon\varepsilon_0 v_f d_z E, \quad d_z J = 0, \tag{10}$$

$$d_z E = \frac{q}{\varepsilon\varepsilon_0}[\rho + N_d]. \tag{11}$$

The velocity of the negative front v_f cannot be smaller than the saturated electron velocity v_{ns}.[2,12] As we will see in the next section, a constant velocity v_f=constant implies a time-independent total current density J=constant.

C. Relation between the current density and the front velocity

Using Eq. (11) to eliminate $d_z E$ from Eq. (10), we find

$$d_z J = 0,$$

$$J = q v_f N_d + qj,$$

$$j \equiv v^+\sigma + [v_f + v^-]\rho. \tag{12}$$

Here, j is chosen to be a particle current density whereas J is a charge current density. Both J and j are constants in space. Typically the electric field at the left boundary $E_{\text{left}} \equiv E(x=0)$ is too low for impact ionization $[\alpha_{n,p}(E_{\text{left}})=0]$ but sufficiently strong to saturate the drift velocities so that $v_n(E_{\text{left}})=v_{ns}$, $v_n(E_{\text{left}})=v_{ps}$ (see Fig. 1). Then, j is determined by small concentrations n_0, $p_0 \ll N_d$ of free carriers that are present during the front passage in the depleted part of the structure far away from the ionization zone,

$$j = v_s^+\sigma_0 + [v_f + v_s^-]\rho_0,$$

$$\sigma_0 \equiv n_0 + p_0,\ \rho_0 \equiv p_0 - n_0,\ v_s^+ \equiv \frac{v_{ns}+v_{ps}}{2},\ v_s^- \equiv \frac{v_{ps}-v_{ns}}{2}. \tag{13}$$

Since σ_0, $\rho_0 \ll N_d$ and the second term in Eq. (12) is negligible. Hence $J \approx qN_d v_f$. This result is well known[2] and physically clear: since the front propagates with velocity v_f into a charged medium with space-charge density qN_d, the current density $qN_d v_f$ is required to neutralize the space charge of the ionized donors. Hence for a planar front, self-similar propagation with constant velocity v_f corresponds to a fixed total current in the external circuit $d_t J=0$.

Although the initial carrier density in the depleted region is low, $\sigma_0 \ll N_d$, its presence is a requirement for the front to propagate with a velocity v_f that exceeds the electron drift velocity v_{ns}. This fast propagation mode is possible because these initial carriers multiply in an avalanchelike manner as soon as the electric field exceeds the ionization threshold.

In the case under study the concentrations n_0 and p_0 are not permanently nonvanishing in the medium the front propagates into. On the contrary, a certain mechanism creates these carriers in the n base just before the front starts to travel, and it actually triggers this propagation. This mechanism is not universal and depends on the specific design and operation mode of a semiconductor device. In microwave TRAPPAT diodes the carriers that remain in the structure from the previous front passage serve as initial carriers for the next passage.[12] In contrast, in high-voltage diodes used as pulse sharpeners the time period between subsequent front passages is so long (typically > 100 μs) that each front passage represents an independent event.[3–5] Between the pulses the reverse voltage is kept close to the stationary breakdown voltage u_b. During this waiting period, which can be arbitrarily long, the leakage current is much smaller than qj, so that n base is essentially empty. To trigger the front the applied voltage u is being rapidly increased above u_b. Experiments show that the front starts to travel when u exceeds u_b several times.[3–5] It appears that in these devices the initial carriers are generated by field-enhanced ionization of deep-level electron traps.[23–25] The release of electrons bound on these deep centers triggers the front and provides conditions for its superfast propagation.[26] Here, we focus exclusively on the stage when the ionization front is already traveling and refer to Refs. 24 and 25 for the detailed discussion on triggering and initial carriers problems. We assume that concentration of initial carriers suffices for using our density model and we treat σ_0 as an input parameter of our model.

D. Final set of equations

Equation (12) allows us to express the "space charge" ρ via the total concentration σ as

$$\rho = -\frac{v^+(E)}{v_f + v^-(E)}\sigma + \frac{j}{v_f + v^-(E)}, \qquad d_z j = 0. \tag{14}$$

Substituting Eq. (14) in Eq. (9), we obtain the final differential equation for σ,

$$d_z\left[\frac{(v_f+v^-)^2 - (v^+)^2}{v_f+v^-}\sigma + \frac{v^+}{v_f+v^-}j\right] = 2G. \tag{15}$$

The impact ionization can be expressed via variables σ and ρ as

$$G(\sigma,\rho,E) = \beta^+(E)\sigma + \beta^-(E)\rho, \tag{16}$$

with impact ionization frequencies

$$\beta^\pm \equiv \frac{v_p(E)\alpha_p(E) \pm v_n(E)\alpha_n(E)}{2}. \tag{17}$$

Using Eq. (14) again to exclude ρ, we obtain

$$G(\sigma,E) = \beta_{\text{eff}}(E,v_f)\sigma + \frac{\beta^-}{v_f+v^-}j,$$

$$\beta_{\text{eff}}(E,v_f) \equiv \frac{\beta^+[v_f+v^-] - \beta^- v^+}{v_f+v^-}. \tag{18}$$

Finally, we express ρ by σ in the Poisson equation, Eq. (11). This leads to Eq. (20) below.

The two equations for the total carrier concentration σ and the field E,

$$d_z\left[\frac{(v_f+v^-)^2 - (v^+)^2}{v_f+v_-}\sigma + \frac{v^+}{v_f+v^-}j\right] = 2\beta_{\text{eff}}(E,v_f)\sigma + \frac{2\beta^-}{v_f+v^-}j, \tag{19}$$

Downloaded 11 Mar 2010 to 131.155.151.137. Redistribution subject to AIP license or copyright; see http://jap.aip.org/jap/copyright.jsp

$$d_z E = b - \frac{q}{\varepsilon\varepsilon_0}\frac{v^+}{v_f + v^-}\sigma,$$

$$b \equiv \frac{q}{\varepsilon\varepsilon_0}\left(N_d + \frac{j}{v_f + v^-}\right), \tag{20}$$

with the known functions $v^{\pm}(E)$, $\beta^{\pm}(E)$, and $\beta_{\mathrm{eff}}(E,v_f)$ and the constant

$$j \equiv v^+\sigma + [v_f + v^-]\rho, \tag{21}$$

completely describe the self-similar propagation of impact ionization front.

Summarizing, we have first substituted the variables (n,p,E) by the new variables (σ,ρ,E), and then we have expressed ρ by the conserved total current J (or j) and σ. In this way we have eliminated the third equation from the original set Eq. (1) using the fact that the local space-charge density ρ is no independent variable when the conserved total current J and the local carrier density σ and field E are fixed. The form of the final equations, Eqs. (19) and (20), is one of two ordinary differential equations of first order.

E. Special and limiting cases

Apart from the general case $v_n(E) \neq v_p(E)$, $\alpha_n(E) \neq \alpha_p(E)$, it is instructive to consider the following special cases:

(a) $v_n(E) = v_p(E) \equiv v(E), \quad \alpha_n(E) = \alpha_p(E) \equiv \alpha(E),$

(b) $v_n(E) = v_p(E) \equiv v(E), \quad \alpha_p(E) = 0, \quad \alpha_n(E) \equiv \alpha(E),$

(c) $v_n(E) = v_p(E) \equiv v(E), \quad \alpha_n(E) = 0, \quad \alpha_p(E) \equiv \alpha(E).$

In case (a) electrons and holes are fully equal, in cases (b) and (c) their drift velocities are equal, but impact ionization takes place due to only one type of carriers. For example, cases (b) and (c) are simplified but reasonable approximations for Si and SiC,[27] respectively.

Another two limiting cases provide insight into the front dynamics for materials where the asymmetry between positive and negative carriers is very strong,

(d) $v_n(E) \equiv v(E), \quad v_p(E) = 0, \quad \alpha_n(E) \equiv \alpha(E), \quad \alpha_p = 0,$

(e) $v_p(E) \equiv v(E), \quad v_n(E) = 0, \quad \alpha_p(E) \equiv \alpha(E), \quad \alpha_n = 0.$

Below we refer to these special cases as cases (a), (b), (c), (d), and (e); we also use these labels to denote the respective curves in the figures.

III. GENERAL PROPERTIES OF THE STATIONARY FRONT PROPAGATION

The main parameters of the traveling front are the maximum electric field E_m, the width ℓ_ρ of the screening region, the voltage u across the n base, the carrier concentration σ_{pl}, and electric field E_{pl} in the electron-hole plasma behind the front (Fig. 1). [In Fig. 2 we sketch the respective $\sigma(E)$ dependence that follows from $E(x)$ and $\sigma(x)$ dependences shown in Fig. 1.] In this section we relate these parameters to the front velocity v_f, the doping level N_d, and the initial

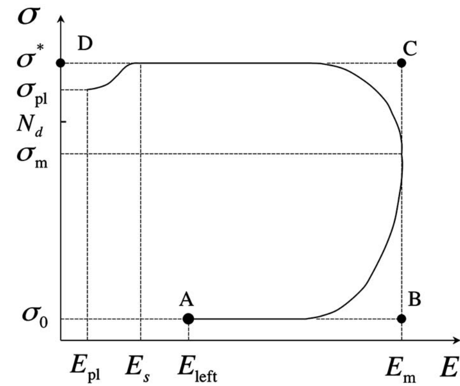

FIG. 2. Dependence of total carrier concentration on electric field $\sigma(E)$ in the traveling ionization front. See notations and comments to Fig. 1. Path A–B–C–D corresponds to piecewise linear approximation of the field profile shown in Fig. 10.

concentration σ_0 in the deleted region, assuming that v_f =constant and front propagation is self-similar. Note that according to Eq. (12), the velocity v_f can be expressed by the current density $J = qN_d v_f$.

A. Ordering of scales

In semiconductors the drift velocities $v_{n,p}(E)$ typically saturate in electric fields above the characteristic fields $E_{ns,ps}$ that are much smaller than the effective threshold of impact ionization. Consequently, in the range of electric fields where impact ionization sets in $(\alpha_{n,p} \neq 0)$ the velocities of free carriers do not depend on electric field $[v^+(E) = v_s^+,\ v^-(E) = v_s^-$ in Eqs. (19)–(21)]. On the other hand, the generation term is negligible in the range of electric fields where the nonlinearity of $v_{n,p}(E)$ dependencies is essential.

For semiconductors where the drift velocities $v_{n,p}(E)$ depend monotonically on the field, the approximations

$$v_n(E) = v_{ns}\frac{E}{E + E_{ns}}, \quad v_p(E) = v_{ps}\frac{E}{E + E_{ps}}, \tag{22}$$

and their modifications are widely used.[28] The impact ionization coefficients for electrons and holes are usually modeled as[29]

$$\alpha_n(E) = \alpha_{n0}\exp(-E_{n0}/E),$$

$$\alpha_p(E) = \alpha_{p0}\exp(-E_{p0}/E). \tag{23}$$

This approximation is known as the Townsend approximation in gas discharge physics.[30] The characteristic transport fields $E_{ns,ps}$ are typically much smaller than the impact ionization fields $E_{n0,p0}$: $E_{ns,ps} \ll E_{n0,p0}$. For example, in Si we have $E_{ns,ps} \sim 10^4$ V/cm, whereas $E_{n0,p0} \sim 10^6$ V/cm.[27] It should be noted that none of these explicit approximations Eq. (22) or Eq. (23) is needed for our analytical results.

Equations (19)–(21) will be solved separately in the range of strong electric fields $E_s < E \lesssim E_0$ where impact ionization takes place and the range of moderate-to-low electric field $E \lesssim E_s$ where transition from high-field transport to low-field transport occurs and the plasma layer is formed. Due to the overlap between these two regions the obtained solutions can be sewn together, providing a consistent description.

Downloaded 11 Mar 2010 to 131.155.151.137. Redistribution subject to AIP license or copyright; see http://jap.aip.org/jap/copyright.jsp

B. Equations in the high-field region

For $E>E_{ns,ps}$ we assume that carriers drift with constant velocities $v_{n,p}(E)=v_{ns,ps}$. Then, Eqs. (19)–(21) become

$$d_z\sigma=\lambda\beta_{\text{eff}}(E,v_f)\sigma, \tag{24}$$

$$d_zE=b-c\sigma, \tag{25}$$

$$j=v_s^+\sigma+(v_f+v_s^-)\rho, \tag{26}$$

where

$$\lambda\equiv\frac{2(v_f+v_s^-)}{(v_f+v_s^-)^2-(v_s^+)^2},$$

$$b\equiv\frac{q}{\varepsilon\varepsilon_0}\left(N_d+\frac{j}{v_f+v_s^-}\right)\approx\frac{qN_d}{\varepsilon\varepsilon_0},$$

$$c\equiv\frac{q}{\varepsilon\varepsilon_0}\frac{v_s^+}{v_f+v_s^-},$$

$$v_s^\pm\equiv\frac{v_{ps}\pm v_{ns}}{2}. \tag{27}$$

The coefficients λ, b, and c are constants. When deriving Eq. (24) from Eq. (19) we neglect the second term on the right-hand side. This is justified because the order of magnitude value of this term is $\beta^-(v_s^+/v_f)\sigma_0$, which is much smaller than the first term. We also take into account that $j/(v_f+v^-)\sim(v_s/v_f)\sigma_0\ll N_d$ in the expression for b.

C. Carrier concentration just behind the ionization zone

At the point x_f where electric field reaches the maximum value E_m the slope of electric field profile is equal to zero (see Fig. 1). In the comoving frame x_f corresponds to the point $z_m=x_f+v_ft$ that does not vary in time. It follows from $d_zE=0$ and Eq. (25) that

$$\sigma_m\equiv\sigma(z_m)=\frac{b}{c}=\frac{v_f+v_s^-}{v_s^+}N_d+\frac{j}{v_s^+}\approx\frac{v_f+v_s^-}{v_s^+}N_d. \tag{28}$$

Dividing Eq. (24) by Eq. (25) we exclude z, and then employ Eq. (28). This yields

$$\frac{\sigma_m-\sigma}{\sigma}d\sigma=\frac{\lambda}{c}\beta_{\text{eff}}(E,v_f)\text{d}E. \tag{29}$$

Let us denote as $\sigma^\star$ the concentration σ which is reached just behind the ionization zone (Fig. 1). Then, the integrals of the left-hand side of Eq. (29) from σ_0 to σ_m and from $\sigma^\star$ to σ_m are both equal to the integral of the right-hand side from 0 to E_m (see Fig. 2),

$$\int_{\sigma_0}^{\sigma_m}\frac{\sigma_m-\sigma}{\sigma}\,\text{d}\sigma=\int_{\sigma_\star}^{\sigma_m}\frac{\sigma_m-\sigma}{\sigma}\,\text{d}\sigma=\frac{\lambda}{c}\int_0^{E_m}\beta_{\text{eff}}(E,v_f)\text{d}E. \tag{30}$$

Taking integrals over σ, we find the relation between the concentration behind the front $\sigma^\star$, front velocity v_f/v_s, the doping level N_d, and initial concentration σ_0,

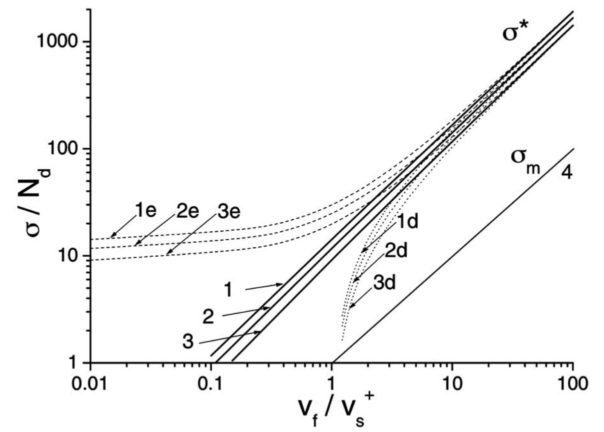

FIG. 3. Concentration $\sigma^\star$ just behind the ionization zone as a function of v_f/v_s^+ for different values of σ_0/N_d. Thick solid lines 1, 2, 3 correspond to symmetric case $v_s^-=0$. Dotted lines 1d, 2d, 3d and dashed lines 1e, 2e, 3e correspond to the two limiting asymmetric cases $v_s^-/v_s^+=-1$ [immobile holes, case (d)] and $v_s^-/v_s^+=1$ [immobile electrons, case(e)], respectively. Curves of first, second, and third series correspond to $\sigma_0/N_d=10^{-3}$, 10^{-4}, and 10^{-5}, respectively. Thin solid line 4 shows concentration σ_m at the point of maximum electric field for the symmetric case $v_s^-=0$.

$$\sigma^\star=\sigma_m\ln\frac{\sigma^\star}{\sigma_0}+\sigma_0\approx\sigma_m\ln\frac{\sigma^\star}{\sigma_0}. \tag{31}$$

The concentration $\sigma^\star$ does not depend on β_{eff} and thus not on the specific form of $\alpha_{n,p}(E)$. Equation (28) generalizes Eq. (29) in Ref. 2.

In Fig. 3 we show $\sigma^\star$ and σ_m as functions of v_f/v_s^+ for different values of σ_0/N_d. Solid lines 1, 2, 3 correspond to the symmetric case $v_s^-=0$. These dependencies are valid for all three special cases (a), (b), and (c) (see Sec. II E) if v_s^+ is replaced by v_s. We see that $\sigma^\star$ is approximately 10 times larger than σ_m (line 4), whereas σ_m exceeds σ_0 by several orders of magnitude. Dashed lines 1d, 2d, 3d and dotted lines 1e, 2e, 3e show $\sigma^\star$ for two extreme asymmetric cases $v_s^-/v_s^+=\mp1$ that correspond to immobile holes [case (d), $v_{ps}=0$] and immobile electrons [case (e), $v_{ns}=0$], respectively. In the case (d) of immobile holes $\sigma^\star\to0$ when $v_f/v_s^+\to1$ (although the part $v_f<2v_s^+=v_{ns}$ is unphysical). In contrast, in the case (e) of immobile electrons $\sigma^\star$ practically does not depend on v_f for $v_f/v_s^+<1$. This plateau exists for $v_s^->0$ and corresponds to the interval of front velocities $v_{ns}<v_f<v_{ps}$ (recall that for negative front $v_f\geq v_{ns}$). Even for the limiting cases $v_s^-/v_s^+=\mp1$ the effect of transport asymmetry is small for $v_f/v_s^+>10$. Actual values of $|v_s^-/v_s^+|$ are much smaller: at room temperatures we have $v_s^-/v_s^+\approx-0.1$, -0.05, and -0.3 for Si, GaAs, and SiC, respectively.[27]

According to Eq. (26) the space charge of free carriers behind the ionization zone $\rho^\star$ is proportional to $\sigma^\star$,

$$\rho^\star=-\frac{v_s^+}{v_f+v_s^-}\sigma^\star+\frac{j}{v_f+v_s^-}\approx-\frac{v_s^+}{v_f+v_s^-}\sigma^\star. \tag{32}$$

Electron and holes concentrations $n^\star,p^\star=(\sigma^\star\mp\rho^\star)/2$ are recovered as

$$n^\star=\frac{v_f+v_{ps}}{2v_f+v_{ps}-v_{ns}}\sigma^\star,$$

Downloaded 11 Mar 2010 to 131.155.151.137. Redistribution subject to AIP license or copyright; see http://jap.aip.org/jap/copyright.jsp

$$p^\star = \frac{v_f - v_{ns}}{2v_f + v_{ps} - v_{ns}}\sigma^\star. \tag{33}$$

The appearance of negative space charge $\rho^\star = p^\star - n^\star < 0$ is a combined effect of spatially inhomogeneous ionization and separation of electrons and holes in strong electric field.

D. Maximum electric field

The maximum field E_m is determined by integrating Eq. (29),

$$\int_0^{E_m} \beta_{\text{eff}}(E)\text{d}E = \frac{b}{\lambda}\left(\ln\frac{\sigma_m}{\sigma_0} - 1 + \frac{\sigma_0}{\sigma_m}\right). \tag{34}$$

Substituting the expressions for $\beta_{\text{eff}}(E)$, λ, b, and σ_m, we obtain the explicit formula

$$\frac{v_s^+ - v_s^-}{v_f + v_s^- - v_s^+}\int_0^{E_m} \alpha_n(E)\text{d}E + \frac{v_s^+ + v_s^-}{v_f + v_s^- + v_s^+}\int_0^{E_m} \alpha_p(E)\text{d}E = \frac{qN_d}{\varepsilon\varepsilon_0}\left[\ln\left(\frac{v_f + v_s^-}{v_s^+}\frac{N_d}{\sigma_0}\right) - 1\right]. \tag{35}$$

Straightforward numerical integration of Eq. (35) for given dependencies $\alpha_{n,p}(E)$ makes it possible to determine E_m as a function of v_f and σ_0/N_d for any semiconductor material.

For the special cases (a), (b), (c), (d), and (e) (see Sec. II E) and the Townsend's dependence $\alpha(E) = \alpha_0 \exp(-E_0/E)$, Eq. (35) yields

$$\int_0^{E_m/E_0} \exp(-1/y)\text{d}y = \frac{E^\star(v_f/v_s, \sigma_0/N_d, \alpha_0)}{E_0}, \tag{36}$$

$$E^\star \equiv \frac{b}{\alpha_0}\frac{v_f^2 - v_s^2}{2v_f v_s}\left[\ln\left(\frac{v_f}{v_s}\frac{N_d}{\sigma_0}\right) - 1\right] \quad \text{for case (a)}, \tag{37}$$

$$E^\star \equiv \frac{b}{\alpha_0}\frac{v_f \mp v_s}{v_s}\left[\ln\left(\frac{v_f}{v_s}\frac{N_d}{\sigma_0}\right) - 1\right] \quad \text{for cases (b) and (c)}, \tag{38}$$

$$E^\star \equiv \frac{b}{\alpha_0}\frac{v_f \mp v_s}{v_s}\left[\ln\left(\frac{2v_f \mp v_s}{v_s}\frac{N_d}{\sigma_0}\right) - 1\right] \quad \text{for cases (d) and (e)}. \tag{39}$$

The dimensional coefficient b/α_0 in $E^\star$ has a meaning of change of the electric field on the length of impact ionization α_0^{-1} for the slope $d_z E = b$ which is determined by the doping level N_d. For realistic parameters $b/\alpha_0 \ll E_0$. Comparing Eq. (38) with Eq. (39), we see that asymmetry of transport properties has a logarithmically weak effect on E_m.

We solve Eq. (36) numerically and show $E_m/E^\star$ as a function of $E_0/E^\star$ in Fig. 4. Together with Eqs. (37)–(39), this dependence makes it possible to determine E_m for given values of v_f/v_s, σ_0/N_d, α_0, and E_0 for the special cases (a)–(e). [Note that $E_m/E^\star \to 1$ when $E_0/E^\star \to 0$. This limit corresponds to ultrastrong electric field when $\alpha(E) \to \alpha_0$.] E_m increases with E_0 because the effective threshold of impact ionization becomes higher.

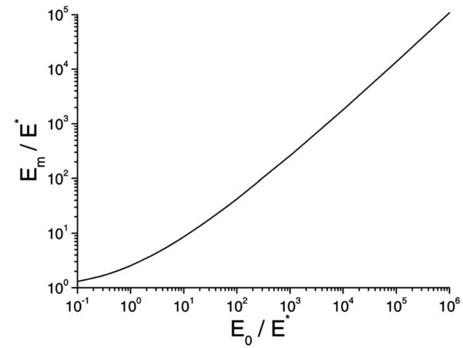

FIG. 4. Maximum electric field E_m as a function of E_0 according to Eq. (36). Both E_m and E_0 are normalized by $E^\star(v_f/v_s, \sigma_0/N_d, \alpha_0)$. Note that $E_m/E^\star \to 1$ when $E_0/E^\star \to 0$.

In Fig. 5 we show E_m as a function of v_f/v_s for different values of σ_0/N_d. Thick solid lines 1a, 2a, 3a correspond to the symmetric case (a) [Eq. (37)], thin solid lines 1b, 2b, 3b and dashed lines 1c, 2c, 3c correspond to the cases of "monopolar ionization" (b) and (c) [Eq. (38)], respectively. E_m is the smallest for the symmetric case $\alpha_n = \alpha_p$ because both types of carriers are involved in impact ionization. Curves 1c, 2c, 3c are "discontinuous;" E_m tends to a finite value when $v_f/v_s \to 1$, whereas we expect $E_m = 0$ for $v_f/v_s = 1$ as it is for the curves 1a, 2a, 3a and 1b, 2b, 3b. This feature results from the assumption $\alpha_n = 0$ and disappears for arbitrary small but nonzero value of α_n. Physically it means that impact ionization by electrons that move parallel to the front is important at low front velocities $v_f \sim v_s$ even in the case $\alpha_n \ll \alpha_p$. The curves for two types of monopolar ionization (b) and (c) become close with increase of v_f. The dependencies $E(v_f)$ calculated for fully immobile holes or electrons [cases (d) and (e), Eq. (39), the respective curves not shown] turn out to be very close to the cases of monopolar ionization (b) and (c) [Eq. (38)], curves 1b, 2b, 3b and 1c, 2c, 3c, respectively]: the difference is smaller than 2% in the whole interval $1 < v_f/v_s < 100$. It means that E_m is much more influenced by the asymmetry of impact ionization coefficients than by the asymmetry of drift velocities. We also see that E_m and hence the effective width of ionization zone ℓ_f decrease with σ_0. This observation explains why the concentration $\sigma^\star$ (see Fig. 3) also decreases with σ_0. In Fig. 5 we choose $b/(\alpha_0 E_0) = 0.0002$. For Si this value corresponds to $N_d = 10^{14}$ cm^{-3}, which is a typical doping level for high-voltage Si structures.[3–5] Since in Si impact ionization by electrons dominates and $v_{ns} \approx v_{ps}$ (Ref. 27), curves 1b, 2b, and 3b provide a good approximation for this material.

Figure 6 shows the dependence $E_m(v_f)$ for different values of $b/(\alpha_0 E_0)$ and the fixed value of σ_0/N_d. E_m increases with N_d due to the decrease of the effective width of ionization zone ℓ_f and decreases with α_0 due to the more efficient impact ionization.

The $E_m(v_f)$ dependences obtained for the case of symmetric ionization $\alpha_n = \alpha_p$ and ionization by electrons (curves 1a, 2a, 3a and 1b, 2b, 3b in Figs. 5 and 6) can be fitted by the square-root function

Downloaded 11 Mar 2010 to 131.155.151.137. Redistribution subject to AIP license or copyright; see http://jap.aip.org/jap/copyright.jsp

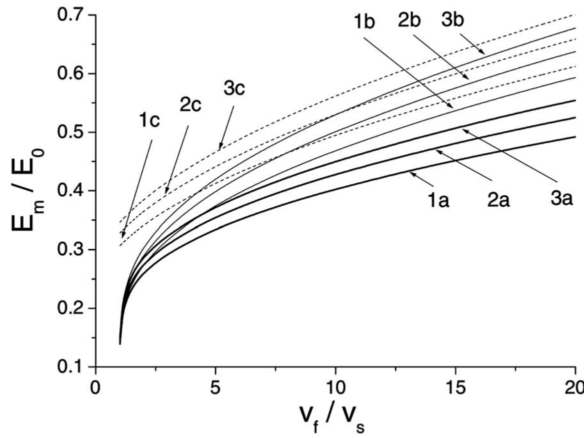

FIG. 5. Maximum electric field E_m as a function of v_f/v_s for different values of σ_0/N_d according to Eq. (36). Thick solid curves 1a, 2a, 3a correspond to the symmetric case (a) $\alpha_n(E)=\alpha_p(E)$, $v_{ns}=v_{ps}$ [Eq. (37)]. Thin solid curves 1b, 2b, 3b correspond to impact ionization by electrons $\alpha_p(E)=0$, $v_{ns}=v_{ps}$ [case (b), Eq. (38)]; dashed curves 1c, 2c, 3c correspond to impact ionization by holes $\alpha_n(E)=0$, $v_{ns}=v_{ps}$ [case (c), Eq. (38)]. Curves of first, second, and third series correspond to $\sigma_0/N_d=10^{-3}$, 10^{-4}, and 10^{-5}, respectively. The parameter $b/(\alpha_0 E_0)=0.0002$ corresponds to the doping level $N_d=10^{14}$ cm^{-3} in Si.

$$E_m(v_f) - E_{\rm th} \sim E_0\sqrt{(v_f/v_s) - 1}, \tag{40}$$

where $E_{\rm th}\approx 0.15,\ldots,0.2E_0$ plays the role of the effective threshold of impact ionization. This fit is quantitatively accurate for $v_f/v_s>2$ and remains qualitatively correct for $1<v_f/v_s<2$. Straightforward examination of Eq. (35) shows that the square-root dependence corresponds to the piecewise linear approximation of the impact ionization coefficient $\alpha(E)$,

$$\alpha(E) \sim (E - E_{\rm th})\Theta(E - E_{\rm th}), \tag{41}$$

where $\Theta(E)$ is the step function. The function Eq. (41) approximates the Townsend's dependence $\alpha(E)=E_0 \exp(-E_0/E)$ reasonably well in the most important interval of electric fields $0.3,\ldots,0.7E_0$ (see the inset to Fig. 6). [Previously the approximation Eq. (41) has been discussed in the theory of fingerlike streamers in Ref. 30.] It is remarkable that the dynamics of ionization fronts reveals the existence of effective threshold electric field $E_{\rm th}\approx 0.2E_0$ in spite of the absence of any kind of cutoff at low electric fields in the Townsend's dependence itself. In particular, the square-root dependence Eq. (40) implies that $v_f\sim \ell_f^2$ if we define $\ell_f \approx (E_m-E_{\rm th})/b$.

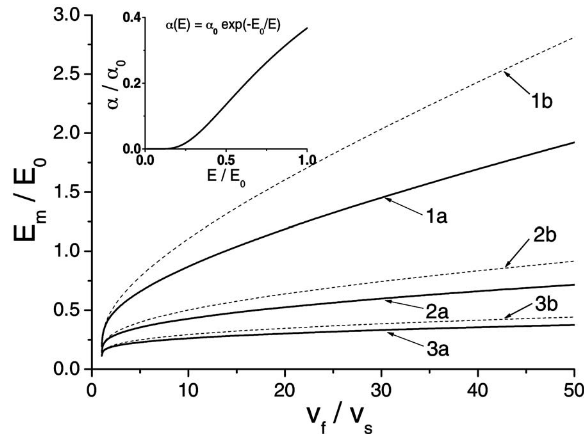

FIG. 6. Maximum electric field E_m as a function of v_f/v_s for different values of $b/(E_0\alpha_0)$ according to Eq. (36). Thick solid lines 1a, 2a, 3a correspond to the symmetric case $\alpha_n(E)=\alpha_p(E)$, $v_{ns}=v_{ps}$ [case (a), Eq. (37)]. Thin solid lines 1b, 2b, 3b correspond to impact ionization by electrons $\alpha_p(E)=0$, $v_{ns}=v_{ps}$ [case (b), Eq. (38)]. Curves of first, second, and third series correspond to $b/(\alpha_0 E_0)=2\times 10^{-5}$, 2×10^{-4}, and 2×10^{-3}, respectively; $\sigma_0/N_d=10^{-4}$. Inset shows the Townsends's dependence for impact ionization coefficient $\alpha(E)$.

E. Width of the screening region

The screening region is situated just behind the ionization zone (Fig. 1). Here, the electric field is insufficient for impact ionization, but the drift velocities remain saturated. According to Eqs. (19) and (21) in this interval of electric fields the concentration σ and space charge ρ are conserved and maintain values $\sigma^\star$ and $\rho^\star$ determined by Eqs. (31) and (32). The slope of electric field in this region is determined as

$$d_z E = \frac{q}{\varepsilon\varepsilon_0}(\rho^\star + N_d).$$

Taking into account Eqs. (28) and (31), we find the ratio between the slope $|d_z E|$ in the screening region and the slope b in the depleted region,

$$\frac{|d_z E|}{b} = \frac{v_s^+}{v_f + v_s^-}\frac{\sigma^\star}{N_d} - 1 = \ln\frac{\sigma^\star}{\sigma_0} - 1. \tag{42}$$

The width ℓ_ρ of the screening region can be evaluated as

$$\ell_\rho \approx \frac{E_m}{|d_z E|} = \frac{E_m}{b[\ln(\sigma^\star/\sigma_0) - 1]}. \tag{43}$$

Calculating ℓ_ρ in this way, we include in it a part of the ionization zone (see Fig. 1) and hence somewhat overestimate the actual width of the screening region. On the other hand, Eq. (43) gives an idea of the effective front width since it accounts for the two regions of most dramatic change in concentration and electric field: the region of most rapid increase of concentration from E_m to the final value $\sigma^\star$ (by approximately one order of magnitude) and the region of steep drop of electric field from E_m to $E_{\rm pl}\ll E_m$.

We show $|d_z E|/b$ as a function of v_f/v_s^+ in Fig. 7. Solid lines correspond to the symmetric case $v_s^-=0$ for different values of σ_0. These curves correspond also to the special cases (a), (b), and (c) if v_s^+ is replaced by v_s. The electric field profile in the screening region is approximately 10–20 times steeper than in the depleted region. The slope $|d_z E|/b$ has a weak logarithmic dependence on v_f and decreases with σ_0/N_d. Dashed lines and dotted lines represent $|d_z E|/b$ for two limiting asymmetric cases $v_s^-/v_s^+=-1$ [case (d), immobile holes] and $v_s^-/v_s^+=1$ [case (e), immobile electrons]. Similar to $\sigma^\star$, $|d_z E|/b$ has a weak dependence on the asymmetry of saturated drift velocities ($v_s^-\neq 0$) for sufficiently large v_f.

Downloaded 11 Mar 2010 to 131.155.151.137. Redistribution subject to AIP license or copyright; see http://jap.aip.org/jap/copyright.jsp

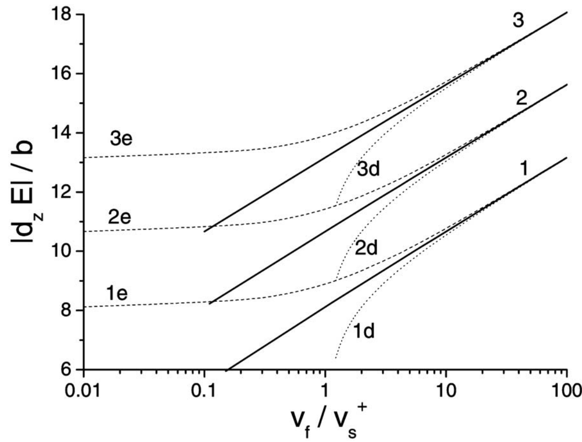

FIG. 7. Slope of electric field in the screening region $|d_zE|$ normalized by the slope in the depleted region $b=qN_d/\varepsilon\varepsilon_0$ as a function of v_f/v_s^+ for different values of σ_0/N_d. Solid lines 1, 2, 3 correspond to the symmetric case $v_s^-=0$. Dotted lines 1d, 2d, 3d and dashed lines 1e, 2e, 3e correspond to the two limiting asymmetric cases $v_s^-/v_s^+=-1$ [immobile holes, case (d)] and $v_s^-/v_s^+=+1$ [immobile electrons, case (e)], respectively. Curves of first, second, and third series correspond to $\sigma_0/N_d=10^{-3}$, 10^{-4}, and 10^{-5}, respectively.

F. Transition from high-field to low-field region

In the region where electric field is insufficient for impact ionization, it follows from Eq. (19) that

$$\frac{[v_f+v^-(E)]^2-[v^+(E)]^2}{v_f+v^-(E)}\sigma+\frac{v^+(E)}{v_f+v^-}j=\text{const}, \qquad (44)$$

where the second small term is negligible. Employing conservation of this quantity, we find explicit expressions for σ and ρ,

$$\sigma(E)=\frac{[v_f^2+v_s^-]^2-[v_s^+]^2}{[v_f^2+v^-(E)]^2-[v^+(E)]^2}\frac{v_f+v^-(E)}{v_f+v_s^-}\sigma^\star,$$

$$\rho(E)=-\frac{v^+(E)}{v_f+v_s^-}\frac{[v_f^2+v_s^-]^2-[v^+(E)]^2}{[v_f^2+v^-(E)]^2-[v^+(E)]^2}\sigma^\star. \qquad (45)$$

For the special cases (a), (b), and (c), this yields

$$\sigma(E)=\frac{v_f^2-v_s^2}{v_f^2-v^2(E)}\sigma^\star,$$

$$\rho(E)=-\frac{v(E)}{v_f}\frac{v_f^2-v_s^2}{v_f^2-v^2(E)}\sigma^\star. \qquad (46)$$

If $v(E)$ is monotonic, then according to Eq. (46) $|\rho(E)|$ monotonically decreases with decrease of E. The transition to neutral plasma occurs when $|\rho(E)|$ reaches N_d and E reaches a certain constant asymptotic value. In semiconductors with nonmonotonic $v_n(E)$ dependence (e.g., GaAs) with maximum at $\tilde{E}<E_s$, we expect that $|\rho(E)|>|\rho^\star|$ near $\tilde{E}$, but the transition to plasma at lower electric fields occurs in the same way as for monotonic $v(E)$.

G. Parameters of the plasma region

Plasma concentration and electric field in plasma are denoted as $\sigma_{\rm pl}$ and $E_{\rm pl}$, respectively (Fig. 1). Generally, these parameters are determined by Eqs. (21) and (44) together with the neutrality condition $\rho_{\rm pl}=-N_d$.

For the general asymmetric case $v^-(E)\neq 0$ we approximate the drift velocities in plasma by the Ohm law $v_n(E)=\mu_nE$, $v_p(E)=\mu_pE$ [note that for the approximations Eq. (22) $\mu_{n,p}=v_{ns,ps}/E_{ns,ps}$]. This yields

$$\frac{(v_f+v_s^-)^2-(v_s^+)^2}{v_f+v_{-s}}\sigma^\star=\frac{(v_f+\mu^-E_{\rm pl})^2-(\mu^+E_{\rm pl})^2}{v_f+\mu^-E_{\rm pl}}\sigma_{\rm pl}, \qquad (47)$$

$$j=\mu^+\sigma_{\rm pl}E_{\rm pl}+(v_f+\mu^-E_{\rm pl})(-N_d),$$

$$\mu^\pm=\frac{\mu_p\pm\mu_n}{2}. \qquad (48)$$

Expressing $E_{\rm pl}$ via $\sigma_{\rm pl}$ in Eq. (48), neglecting j, and substituting in Eq. (47), we find explicit formulas for $\sigma_{\rm pl}$,

$$\sigma_{\rm pl}=\frac{1}{2}A\sigma^\star\left[1+\sqrt{1+\frac{4N_d}{A\sigma^\star}\left(\frac{N_d}{A\sigma^\star}-\frac{\mu^-}{\mu^+}\right)}\right],$$

$$A\equiv\frac{(v_f+v_s^-)^2-(v_s^+)^2}{v_f(v_f+v_s^-)}, \qquad (49)$$

$$E_{\rm pl}=E_s^+\frac{v_f/v_s^+}{\sigma_{\rm pl}/N_d-\mu^-/\mu^+},$$

$$E_s^+\equiv\frac{v_s^+}{\mu^+}. \qquad (50)$$

Expansion over $N_d/A\sigma^\star$ leads to

$$\sigma_{\rm pl}=A\sigma_\star+\frac{N_d^2}{A\sigma^\star}-\frac{\mu^-}{\mu^+}N_d\approx A\sigma^\star=\frac{(v_f+v_s^-)^2-(v_s^+)^2}{v_f(v_f+v_s^-)}\sigma^\star. \qquad (51)$$

Electron and hole concentrations in plasma region are recovered as

$$n_{\rm pl}=\frac{\sigma_{\rm pl}+N_d}{2},\quad p_{\rm pl}=\frac{\sigma_{\rm pl}-N_d}{2}. \qquad (52)$$

It can be derived easily from the continuity of electron and hole flows that $n^\star>n_{\rm pl}$ and $p^\star<n_{\rm pl}$ [see Eq. (33)]. In contrast, the relation between $\sigma^\star$ and $\sigma_{\rm pl}$ is not universal: $A<1$ when $v_s^-\leq 0$, but $A>1$ for $v_s^->0$ and $v_f>[(v_s^+)^2-(v_s^-)^2]/(v_s^-)^2$. Therefore, according to Eq. (51), $\sigma_{\rm pl}<\sigma^\star$ when $v_{ns}>v_{ps}$ for any v_f. However, for sufficiently large v_f we find that $\sigma_{\rm pl}>\sigma^\star$ when $v_{ns}<v_{ps}$. Next, $A\to 0$ for $v_f\to v_{ns}$ and hence according to Eqs. (49) and (52) $\sigma_{\rm pl}\to N_d$, $n_{\rm pl}\to N_d$, $p_{\rm pl}\to 0$. This is consistent with the condition $v_f>v_{ns}$.

For the special cases (a), (b), and (c) when electron and hole drift velocities are equal it is convenient to use the approximation $v(E)=v_sE/(E+E_s)$ in the whole range of electric fields including plasma. After similar derivations we find

Downloaded 11 Mar 2010 to 131.155.151.137. Redistribution subject to AIP license or copyright; see http://jap.aip.org/jap/copyright.jsp

$$\sigma_{\rm pl} = \sigma^\star \frac{v_f^2 - v_s^2}{2v_f^2}\left[1 + \sqrt{1 + \left(\frac{2v_f^2}{v_f^2 - v_s^2}\frac{N_d}{\sigma^\star}\right)^2}\right], \quad (53)$$

$$E_{\rm pl} = E_s \frac{D}{1-D},$$

$$D \equiv \frac{v_f^2 - v_s^2}{2v_s^2}\left[\sqrt{1 + \left(\frac{2v_f^2}{v_f^2 - v_s^2}\frac{N_d}{\sigma^\star}\right)^2} - 1\right]\ln\frac{\sigma^\star}{\sigma_0}. \quad (54)$$

Expanding over $N_d/\sigma^\star$, we obtain simplified dependencies that are valid when $\sigma^\star \gg N_d$,

$$\sigma_{\rm pl} = \frac{v_f^2 - v_s^2}{v_f^2}\left(\sigma^\star + \frac{v_f^2}{v_f^2 - v_s^2}\frac{N_d^2}{\sigma^\star}\right) \approx \frac{v_f^2 - v_s^2}{v_f^2}\sigma^\star,$$

$$E_{\rm pl} = E_s\left[\frac{v_f^2 - v_s^2}{v_f^2}\ln\frac{\sigma^\star}{\sigma_0} - 1\right]^{-1}. \quad (55)$$

The concentration $\sigma_{\rm pl}$ tends to $\sigma^\star$ with increase of v_f and, similar to $\sigma^\star$, shows quasilinear dependence on v_f for $v_f \gg v_s$. In contrast, the dependence of $E_{\rm pl}$ on v_f is very weak.

The concentration $\sigma_{\rm pl}$ and the electric field $E_{\rm pl}$ are shown in Figs. 8 and 9, respectively. In panels (a) these dependencies are shown for different values of σ_0/N_d. Solid curves 1, 2, 3 correspond to the symmetric case $v_s^-=0$. Dashed curves 1d, 2d, 3d correspond to the limiting case (d) of immobile holes $v_s^-/v_s^+=-1$. Dotted curves 1e, 2e, 3e correspond to the opposite limiting case (e) of immobile electrons $v_s^-/v_s^+=1$. For fast fronts $\sigma_{\rm pl}$ increases with v_f linearly, whereas the electric field is close to $E_{\rm pl} \approx 0.1E_s^+$ and weakly decreases with v_f. In panels (b) $\sigma_{\rm pl}$ and $E_{\rm pl}$ are shown for different values of v_s^-/v_s^+ and μ^-/μ^+. We see that the asymmetry in high-field transport is much more important than the asymmetry in the low-field transport. For $v_s^- > 0$ [curves 4,5,6,7 in Fig. 9(b)] the dependence $\sigma_{\rm pl}(v_f)$ has a kind of plateau and the corresponding dependence $E_{\rm pl}(v_f)$ has a minimum. This occurs in the interval of front velocities $v_{ns} < v_f < v_{ps}$. The plateau on $\sigma_{\rm pl}(v_f)$ is caused by the peculiarity of $\sigma^\star(v_f)$ dependence that has been discussed above in Sec. III C (see also Fig. 3). The nonmonotonic behavior of $E_{\rm pl}(v_f)$ becomes clear if we take into account that, according to Eq. (50) in the symmetric case $E_{\rm pl} \sim v_f/\sigma_{\rm pl}$, $E_{\rm pl}$ decreases and increases when the increase of $\sigma_{\rm pl}$ with v_f is superlinear and sublinear, respectively. Hence, "plateau" on the dependence $\sigma_{\rm pl}(v_f)$ corresponds to a minimum on $E_m(v_f)$.

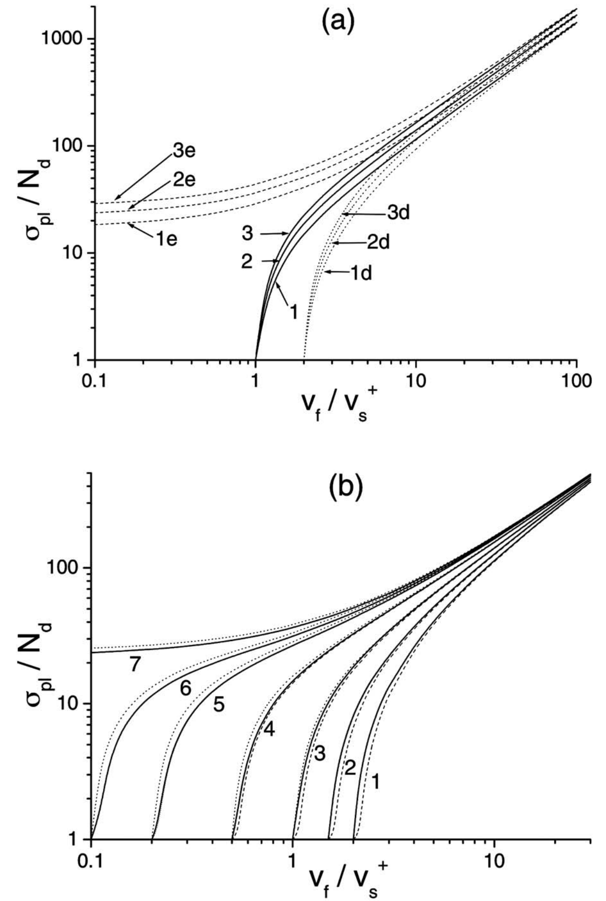

FIG. 8. Concentration of electron-hole plasma $\sigma_{\rm pl}$ generated by the front passage as a function of front velocity v_f. In panel (a) the dependence $\sigma_{\rm pl}(v_f)$ is shown for different values of σ_0/N_d. Solid curves 1, 2, 3 correspond to the case of symmetric transport $v_s^-=0$, $\mu^-=0$ (e.g., $v_{ns}=v_{ps}$, $\mu_n=\mu_p$). Dotted lines 1d, 2d, 3d and dashed lines 1e, 2e, 3e correspond to the limiting cases of immobile holes $v_{ps}=0$, $\mu_p=0$ [case(d)] and immobile electrons $v_{ns}=0$, $\mu_n=0$ [case (e)], and are calculated for the same values of σ_0/N_d. Curves of first, second, and third series correspond to $\sigma_0/N_d=10^{-3}$, 10^{-4}, and 10^{-5}, respectively. In panel (b) the dependence $\sigma_{\rm pl}(v_f)$ is shown for different values of v_s^-/v_s^+ and μ^-/μ^+ and fixed value $\sigma_0/N_d=10^{-4}$. Solid lines from 1 to 7 correspond to $v_s^-/v_s^+=\mu^-/\mu^+=-1$, -0.5, 0, 0.5, 0.8, 0.9, and 1.0, respectively. Associated dotted and dashed lines in panel (b) correspond to $\mu^-/\mu^+=-0.9$ and $\mu^-/\mu^+=0.9$, respectively, and the same value of v_s^-/v_s^+ as for the respective solid lines.

H. Voltage over the structure

The voltage over the structure is given by the integral

$$u = \int_0^W E(x)\mathrm{d}x. \quad (56)$$

We approximate the actual profile $E(z)$ by a piecewise linear profile A–B–C–D shown in Fig. 10, neglecting the voltage drop over the plasma region where the electric field is low. For such profile $\sigma(z)=\sigma_0$ and $d_zE=b-c\sigma_0$ on part A–B, $E=E_m$ and σ increases from σ_0 to $\sigma^\star$ in arbitrary way on part B–C, and $\sigma(z)=\sigma^\star$ and $d_zE=b-c\sigma^\star$ on part C–D. Integration over this profile gives an upper bound for the actual voltage. On the (σ,E) plane this profile corresponds to the rectangular $\sigma(E)$ dependence (dashed line A–B–C–D in Fig. 2). The integral over z can be replaced either by the integral over electric field E or over concentration σ since, according to Eqs. (24) and (25), $\mathrm{d}z=\mathrm{d}E/(b-c\sigma)=\mathrm{d}\sigma/\lambda\beta_{\rm eff}\sigma$. Employing integration over E for branches A–B and C–D and integration over σ for branch B–C, we approximate the integral Eq. (56) as

$$u = \int_{E_{\rm left}}^{E_m}\frac{E\,\mathrm{d}E}{b-c\sigma_0} + \int_{\sigma_0}^{\sigma^\star}\frac{E_m d\sigma}{\lambda\beta_{\rm eff}(E_m)\sigma} + \int_{E_m}^{0}\frac{E\,\mathrm{d}E}{b-c\sigma^\star}. \quad (57)$$

This yields

Downloaded 11 Mar 2010 to 131.155.151.137. Redistribution subject to AIP license or copyright; see http://jap.aip.org/jap/copyright.jsp

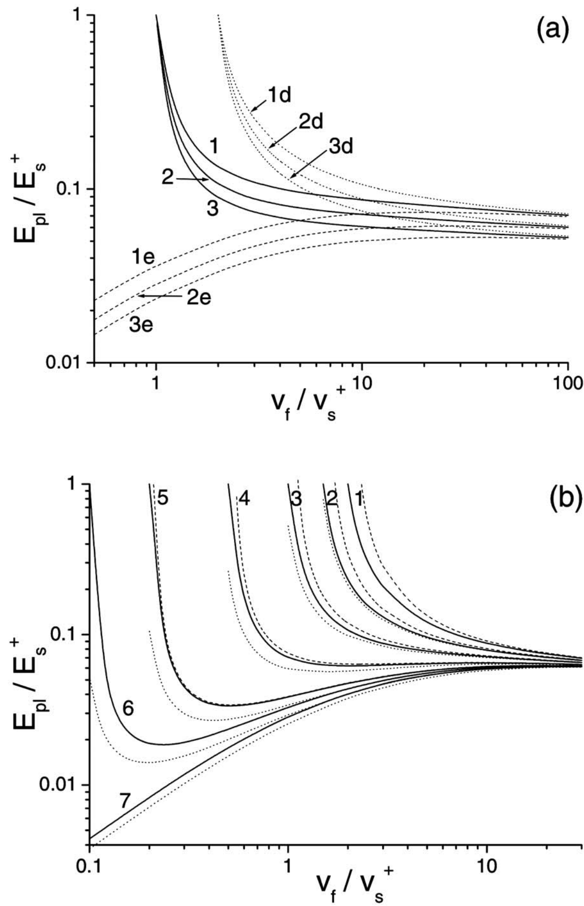

FIG. 9. Electric field $E_{\rm pl}$ in the electron-hole plasma generated by the front passage as a function of front velocity v_f. In panel (a) the dependence $E_{\rm pl}(v_f)$ is shown for different values of σ_0/N_d. Solid curves 1, 2, 3 correspond to case of symmetric transport $v_s^-=0$, $\mu^-=0$ (e.g., $v_{ns}=v_{ps}$, $\mu_n=\mu_p$). Dotted lines 1d, 2d, 3d and dashed lines 1e, 2e, 3e correspond to the limiting cases of immobile holes $v_{ps}=0$, $\mu_p=0$ [case(d)] and immobile electrons $v_{ns}=0$, $\mu_n=0$ [case (e)], respectively. Curves of first, second, and third series correspond to $\sigma_0/N_d=10^{-3}$, 10^{-4}, and 10^{-5}, respectively. In panel (b) the dependence $E_{\rm pl}(v_f)$ is shown for different values of v_s^-/v_s^+ and μ^-/μ^+ and fixed value $\sigma_0/N_d=10^{-4}$. Solid lines from 1 to 7 correspond to $v_s^-/v_s^+=\mu^-/\mu^+=-1$, -0.5, 0, 0.5, 0.8, 0.9, and 1.0, respectively. Associated dotted and dashed lines correspond to $\mu^-/\mu^+=-0.9$ and $\mu^-/\mu^+=0.9$, respectively, and the same value of v_s^-/v_s^+ as for the respective solid lines.

$$u \approx \frac{1}{2c}\left[\frac{E_m^2-E_{\rm left}^2}{\sigma_m-\sigma_0}+\frac{E_m^2}{\sigma^\star-\sigma_m}\right]+\frac{E_m}{\lambda\beta_{\rm eff}(E_m)}\ln\frac{\sigma^\star}{\sigma_0}. \quad (58)$$

Here, the first term corresponds to the contribution of the inclined parts A–B and C–D of the field profile. The second term corresponds to the horizontal part B–C and hence approximates the contribution of the nonlinear part of the profile near its maximum. The ratio of the first term to the second one can be estimated as $v_s\alpha(E_m)\tau_\rho$, where $v_s\alpha(E_m)$ is the frequency of impact ionization, $\tau_\rho \equiv \ell_\rho/v_f$ is the time the front takes to move over its own width ℓ_ρ, and it is assumed that $v_n=v_p$, $\alpha_n=\alpha_p$, $v_f \gg v_s$. [For this estimate we assume $E_m \gg E_{\rm left}$ and employ Eq. (43).] Typically $v_s\alpha(E_m)\tau_\rho \gg 1$ and hence the first term in Eq. (58) dominates over the second one. It means that the nonlinear part of the profile $E(z)$ which is located near its maximum is small, and the typical shape of $E(z)$ is close to triangular.

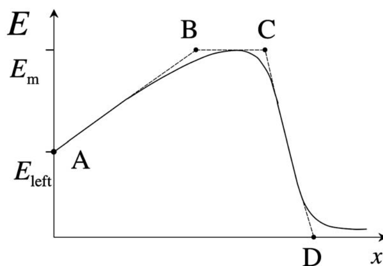

FIG. 10. Piecewise linear approximation of the field profile used to calculate the voltage u across the n base (Sec. III H). The respective $\sigma(E)$ dependence is shown by dashed line A–B–C–D in Fig. 2.

Taking into account that $E_{\rm left}=E_m-bx_f$, we can represent u as

$$u \approx E_m x_f - \frac{bx_f^2}{2}+\frac{E_m^2}{2b[\ln(\sigma^\star/\sigma_0)-1]}+\frac{E_m}{\lambda\beta_{\rm eff}(E_m)}\ln\frac{\sigma^\star}{\sigma_0}. \quad (59)$$

Since the dependencies $\sigma^\star(v_f)$ and $E(v_f)$ are already determined [see Eqs. (31) and (35)], Eq. (59) gives u as a function of front position x_f and velocity v_f.

IV. ULTRAFAST FRONTS ($v_f \gg v_s^+$)

The front velocity v_f is often much higher than v_s.[3–9] In the respective limiting case $v_f/v_s^+ \gg 1$ the effect of transport asymmetry vanishes. As it follows from Eqs. (28), (31), and (51), the concentrations σ_m and $\sigma^\star$ can be presented as

$$\sigma_m = \frac{v_f}{v_s^+}N_d, \quad \sigma^\star = \frac{v_f}{v_s^+}N_d \ln\frac{\sigma^\star}{\sigma_0}. \quad (60)$$

The plasma concentration and electric field in plasma are given by

$$\sigma_{\rm pl} = \left[1-\left(\frac{v_s^+}{v_f}\right)^2\right]\sigma^\star \approx \sigma^\star, \quad E_{\rm pl}=\frac{E_s^+}{\ln(\sigma^*/\sigma_0)}. \quad (61)$$

The maximum field is determined by [see Eq. (34)]

$$\int_0^{E_m}[v_{ns}\alpha_n(E)+v_{ps}\alpha_p(E)]{\rm d}E = \frac{qN_d v_f}{\varepsilon\varepsilon_0}\ln\frac{v_f N_d}{v_s^+\sigma_0}. \quad (62)$$

Let us compare these predictions with the results of an elementary model suggested for a planar ionization front in diode structures in Ref. 17 on the basis of the ideas developed for fingerlike streamers in Ref. 31 and 32. In Ref. 17 it is assumed $v_n=v_p$, $v_f \gg v_s$, $\alpha_p=0$, and $\alpha_n(E)=\alpha_0\Theta(E-E_{\rm th})$, where $\Theta(E)$ is the step function. Under these assumptions the order of magnitude values of v_f and $\sigma_{\rm pl}$ has been evaluated as

$$v_f = \frac{\ell_f}{\tau},$$

$$\tau \equiv \frac{1}{v_s\alpha_0}\ln\frac{\sigma_{\rm pl}}{\sigma_0},$$

$$\ell_f \equiv \frac{E_m-E_{\rm th}}{qN_d/\varepsilon\varepsilon_0},$$

Downloaded 11 Mar 2010 to 131.155.151.137. Redistribution subject to AIP license or copyright; see http://jap.aip.org/jap/copyright.jsp

$$\sigma_{\rm pl} = \frac{\alpha_0 \varepsilon \varepsilon_0 E_m}{q}, \qquad (63)$$

where τ is the time it takes for the front to pass over the width of ionization zone ℓ_f.

For $\alpha_n(E)=\alpha_0\Theta(E-E_{\rm th})$, $\alpha_p(E)=0$, we obtain from Eq. (62)

$$v_f = \frac{\ell_f}{\tilde{\tau}}, \quad \tilde{\tau} = \frac{1}{v_s\alpha_0}\ln\frac{\sigma_m}{\sigma_0}. \qquad (64)$$

Then, it follows from Eqs. (60), (61), and (64) that

$$\sigma_{\rm pl} = \frac{\alpha_0\varepsilon\varepsilon_0(E_m-E_{\rm th})}{q} - \sigma_m \ln\frac{\sigma^\star}{\sigma_m} \approx \frac{\alpha_0\varepsilon\varepsilon_0(E_m-E_{\rm th})}{q}. \qquad (65)$$

Predictions for v_f given by Eqs. (63) and (64) differ in the definition of τ. However, the relative difference $(\tau-\tilde{\tau})/\tau = \ln(\sigma^\star/\sigma_m)/\ln(\sigma^\star/\sigma_0)$ does not exceed 10% (see Fig. 3). Next, according to Eq. (63) $\sigma_{\rm pl}$ is proportional to E_m, whereas more the accurate Eq. (65) predicts proportionality to the difference between E_m and $E_{\rm th}$. Therefore, Eq. (63) overestimates $\sigma_{\rm pl}$. Still, it gives the correct order of $\sigma_{\rm pl}$ since in practice $E_{\rm th}$, E_m, and $|E_{\rm th}-E_m|$ are of the same order of magnitude.

V. NONSTATIONARY PROPAGATION

A. Adiabatic condition

The relations between v_f, E_m, $\sigma_{\rm pl}$, and $E_{\rm pl}$ obtained for J=constant still hold when J varies in time providing that this variation is slow in comparison with inner relaxation times of the traveling front. These times are the Maxwellian relaxation time in plasma behind the front τ_M and the time $\tau_\rho \equiv \ell_\rho / v_f$ the front takes to move over the width of the screening region ℓ_ρ. Indeed, any change of the electric field (and hence the current density) in the n base originates from changes of electric charges in the highly doped p^+ and n^+ layers that serve as effective electrodes (see Fig. 1). Further transfer of electric charge into the n base occurs through the plasma layer and is controlled by τ_M. Redistribution of charges in the traveling screening region at the plasma edge takes time τ_ρ. Thus, the times τ_M and τ_ρ characterize how fast the front relaxes to the steady profile that corresponds to the instant value of the current density. Employing Eq. (43), assuming for simplicity $v_s=v_{ns}=v_{ps}$, $\mu=\mu_n=\mu_p$, and taking into account $v_s=\mu E_s$, we obtain

$$\tau_\rho \equiv \frac{\ell_\rho}{v_f} = \tau_M \frac{E_m}{E_s}\frac{\sigma_{\rm pl}}{\sigma^\star}, \quad \tau_M \equiv \frac{\varepsilon\varepsilon_0}{q\mu\sigma_{\rm pl}}. \qquad (66)$$

We see that τ_ρ is much larger than τ_M and hence it is the time τ_ρ that eventually controls the relaxation of the front profile. Consequently, the adiabatic condition for the variation of current J can be presented as

$$\tau_\rho \frac{{\rm d}(\ln J)}{{\rm d}t} \ll 1. \qquad (67)$$

Below, we show that this condition is typically met for the realistic operation mode of high-voltage diodes used as switches in pulse power applications.

B. Coupling to the external circuit

In practice the device is connected to the voltage source $U(t)$ via a load resistance R. The current density J and the voltage over the structure u are related via Kirchhoff's equation,

$$u(t) + RSJ(t) = U(t). \qquad (68)$$

In high-voltage diodes used in pulse power applications the front passage switches the structure from the nonconducting state to the conducting state. At the moment $t=t_0$, when the front starts to travel, $u \approx U(t_0)$ and $J\approx 0$. The switching time is determined as $\Delta t = W/\langle v_f\rangle$, where W is the n base width and $\langle v_f\rangle$ is the mean value of front velocity (generally, v_f increases during the front passage). The device resistivity after switching is negligible in comparison with the load resistance R. Hence $u(t_0+\Delta t)\approx 0$ and $J(t_0+\Delta t) = U(t_0+\Delta t)/(RS) \approx U(t_0+\Delta t)/(RS)$, where we take into account that variation of U within the time period Δt is small. Then, we estimate the relative variation of the current density as

$$\frac{{\rm d}(\ln J)}{{\rm d}t} \sim \frac{J(t_0+\Delta t)-J(t_0)}{\Delta t J(t_0+\Delta_t)} \sim \frac{1}{\Delta t} = \frac{W}{\langle v_f\rangle}.$$

Substituting this estimate into Eq. (67), we present the adiabatic condition as

$$\frac{\langle v_f\rangle}{v_f}\frac{\ell_\rho}{W} \approx \frac{\ell_\rho}{W} \ll 1. \qquad (69)$$

Equation (69) states that the inner dynamics of the traveling front and the outer dynamics that is controlled by the external circuit can be separated if the effective front width ℓ_ρ is much smaller than the size of the system W. Using Eq. (43), we present Eq. (69) as

$$\frac{E_m}{bW}\frac{1}{\ln(\sigma^\star/\sigma_0)-1} \ll 1. \qquad (70)$$

According to Eq. (42) and Fig. 7, the second term in Eq. (70) has a numerical value in the range 0.05–0.1. Therefore, it is necessary that $E_m/(bW)\sim 1$. The adiabatic conditions Eqs. (69) and (70) are met or nearly met for high-voltage sharpening diodes where $W\sim 100-300$ μm and $\ell_\rho \sim 10-20$ μm, but are not likely to be met for much smaller TRAPATT diodes.

In conclusion, the relations between v_f, E_m, and $\sigma_{\rm pl}$ obtained for the self-similar propagation mode can be used in general case to relate the instant values of these parameters for sufficiently large structures and fast fronts. In this case the voltage $u(v_f,x_f)$ given by Eq. (59) can be substituted into the Kirchhoff equation, Eq. (68). Then, equation ${\rm d}x_f/{\rm d}t = -v_f$ (recall that $v_f>0$ for the front traveling in the negative x direction) together with Eq. (68) represents a set

Downloaded 11 Mar 2010 to 131.155.151.137. Redistribution subject to AIP license or copyright; see http://jap.aip.org/jap/copyright.jsp

of ordinary differential equations that describes the front propagation with the external circuit taken into account.

VI. SUMMARY

Basic parameters of plane impact ionization fronts in reversely biased p^+-n-n^+ structure (Fig. 1) are determined by current density J and concentration of initial carriers σ_0 (regime parameters), doping of the n base N_d (structure parameter), and such material parameters as saturated drift velocities v_{ns} and v_{ps}, low-field mobilities μ_n and μ_p, and electron and hole impact ionization coefficients $\alpha_n(E)$ and $\alpha_p(E)$. The front velocity is given by $v_f \approx J/qN_d$ [Eq. (12)]. The concentration of generated plasma $\sigma_{\rm pl}$ and electric field in plasma $E_{\rm pl}$ determined by Eqs. (28), (31), and (49) does not depend on impact ionization coefficients $\alpha_{n,p}(E)$. Concentration of $\sigma_{\rm pl}$ weakly decreases with initial carrier concentration σ_0 [Fig. 8(a)]. For moderate front velocities $v_f \lesssim 5(v_{ns}+v_{ps})$ the concentration $\sigma_{\rm pl}$ and field $E_{\rm pl}$ are sensitive to the ratio v_{ns}/v_{ps}, whereas the asymmetry in low-field transport $\mu_n/\mu_p \neq 1$ has very little effect [Figs. 8(b) and 9(b)]. For higher front velocities $\sigma_{\rm pl}$ and $E_{\rm pl}$ do not depend on v_{ns}/v_{ps} and μ_n/μ_p [Eq. (61)]: σ increases with v_f quasilinearly, whereas $E_{\rm pl}$ weakly decreases.

General dependence of maximum electric field E_m on v_f is given by Eq. (35). Due to strong nonlinearity of impact ionization coefficients $\alpha_{n,p}(E)$, often only one type of carrier contributes to ionization. In this case the dependence $E_m(v_f)$ can be determined in a simple form for the Townsend's approximation $\alpha(E)=\alpha_0 \exp(-E_0/E)$ and symmetric transport $v_{ns}=v_{ps}$ [see Eq. (36) and Fig. 4]. We reveal the existence of the effective threshold of impact ionization $E_{\rm th} \approx 0.2E_0$ (Figs. 5 and 6) and the squareroot character of the $E_{\rm m}(v_f)$ dependence [Eq. (40)]. Equation (40) implies that $v_f \sim \ell_f^2$, where ℓ_f is the effective width of ionization zone. The square-root dependence fails for slow fronts when $\alpha_n \ll \alpha_p$. E_m increases with E_0 and N_d (Fig. 6) and decreases with σ_0 and α_0 (Figs. 4–6). The width ℓ_ρ of the screening region where electric field falls from E_m to $E_{\rm pl}$ weakly depends on v_f and σ_0 [Eq. (42)]. The slope of the electric field in the screening region is about 10–20 times larger than the slope $qN_d/\varepsilon\varepsilon_0$ in the depleted n base to which the front propagates (Fig. 7).

The voltage over the structure u is determined by the front velocity v_f and the front position x_f [Eq. (58)]. The profile of electric field $E(z)$ is essentially triangular since the nonlinear part near its maximum $E=E_m$ is small.

In the case when the current density J varies in time, the front velocity v_f and the front profile $E(z)$ are nonstationary. The largest inner relaxation time $\tau_\rho=\ell_\rho/v_f$ is the time it takes for the front to travel over the width of the screening region ℓ_ρ [Eq. (66)]. The relations between basic front parameters E, ℓ_ρ, $\sigma_{\rm pl}$, and $E_{\rm pl}$ obtained for J=constant remain valid if temporal variation of J is slow with respect to τ_ρ [Eq. (67)]. For the actual case of the device connected in series with an external load, this adiabatic condition [Eq. (67)] can be presented as $\ell_\rho/W \ll 1$ [Eq. (69)]: inner and outer dynamics can be separated if the ionization front is thin with respect to the n base width W. This condition is met or nearly met for high-voltage sharpening diodes.

For very strong electric fields $E \gtrsim E_0$, the direct band-to-band tunneling (Zener breakdown) must be taken into account. Numerical simulations show that in the presence of this ionization mechanism the character of front propagation substantially changes.[18] The respective fronts have been called tunneling-assisted impact ionization fronts.[18] Recently, the dynamic avalanche breakdown of high-voltage diodes with stationary breakdown voltage $u_b \approx 1.5$ kV at extremely high voltage about 10 kV, which corresponds to electric fields above the threshold of Zener breakdown, has been observed experimentally.[19] The analytical theory of tunneling-assisted impact ionization fronts will be reported separately.

ACKNOWLEDGMENTS

We are grateful to P. Ivanov for critical reading of the manuscript and helpful discussions. This work was supported by the Program of Russian Academy of Sciences, "Power semiconductor electronics and pulse technologies." P.R. thanks A. Alekseev for his hospitality at the University of Geneva and acknowledges support from the Swiss National Science Foundation.

[1] H. J. Prager, K. K. N. Chang, and J. Wiesbord, Proc. IEEE **55**, 586 (1968).
[2] B. C. Deloach and D. L. Scharfetter, IEEE Trans. Electron Devices **ED-20**, 9 (1970).
[3] I. V. Grekhov and A. F. Kardo-Susoev, Sov. Tech. Phys. Lett. **5**, 395 (1979) [Pis'ma Zh. Tekh. Fiz. **5**, 950 (1979)].
[4] I. V. Grekhov, A. F. Kardo-Susoev, L. S. Kostina, and S. V. Shenderey, Electron. Lett. **17**, 422 (1981).
[5] I. V. Grekhov, A. F. Kardo-Susoev, L. S. Kostina, and S. V. Shenderey-,Sov. Tech. Phys. Lett. **26**, 984 (1981) [Zh. Tekh. Phys. **51**, 1709 (1981)].
[6] D. Benzel and M. Pocha, Rev. Sci. Instrum. **56**, 1456 (1985).
[7] Zh. I. Alferov, I. V. Grekhov, V. M. Efanov, A. F. Kardo-Sysoev, V. I. Korol'kov, and M. N. Stepanova,Sov. Tech. Phys. Lett. **13**, 454 (1987) [Pis'ma Zh. Tekh. Fiz. **13**, 950 (1987)].
[8] I. V. Grekhov and V. M. Efanov,Sov. Tech. Phys. Lett. **14**, 929 (1988) [Pis'ma Zh. Tekh. Fiz. **14**, 2121 (1988)].
[9] I. V. Grekhov and V. M. Efanov,Sov. Tech. Phys. Lett. **16**, 645 (1990) [Pis'ma Zh. Tekh. Fiz. **16**, 9 (1990)].
[10] I. V. Grekhov, Solid-State Electron. **32**, 923 (1989).
[11] R. J. Focia, E. Schamiloghu, C. B. Fledermann, F. J. Agee, and J. Gaudet, IEEE Trans. Plasma Sci. **25**, 138 (1997).
[12] M. Levinshtein, J. Kostamovaara, and S. Vainshtein, *Breakdown Phenomena in Semiconductors and Semiconductor Devices* (World Scientific, London, 2005).
[13] P. Rodin, U. Ebert, W. Hundsdorfer, and I. Grekhov, J. Appl. Phys. **92**, 1971 (2002).
[14] Yu. D. Bilenko, M. E. Levinstein, M. V. Popova, and V. S. Yuferev, Sov. Phys. Semicond. **17**, 1156 (1983) [Fiz. Tekh. Poluprovodn. (S.-Peterburg) **17**, 1812 (1983)].
[15] A. F. Kardo-Susoev and M. V. Popova, Sov. Phys. Semicond. **30**, 431 (1996) [Fiz. Tekh. Poluprovodn. (S.-Peterburg) **30**, 803 (1996)].
[16] H. Jalali, R. Joshi, and J. Gaudet, IEEE Trans. Electron Devices **45**, 1761 (1998).
[17] P. Rodin, P. Ivanov, and I. Grekhov, J. Appl. Phys. **99**, 044503 (2006).
[18] P. Rodin, U. Ebert, W. Hundsdorfer, and I. Grekhov, J. Appl. Phys. **92**, 958 (2002).
[19] S. K. Lyubutin, S. N. Rukin, B. G. Slovikovsky, and S. N. Tsyranov, Tech. Phys. Lett. **31**, 196 (2005) [J. Appl. Phys. **31**, 36 (2005)].
[20] *Electric Breakdown in Gases*, edited by J. M. Meek and J. D. Craggs (Wiley, New York, 1978).
[21] *Dynamics of Curved Fronts*, edited by P. Pelcé (Academic, Boston, 1988).
[22] M. S. Cross and P. C. Hohenberg, Rev. Mod. Phys. **65**, 851 (1993).
[23] E. V. Astrova, V. B. Voronkov, V. A. Kozlov, and A. A. Lebedev, Semicond. Sci. Technol. **13**, 488 (1998).
[24] P. Rodin and I. Grekhov, Appl. Phys. Lett. **86**, 243504 (2005).
[25] P. Rodin, A. Rodina, and I. Grekhov, J. Appl. Phys. **98**, 094506 (2005).
[26] Generally, emission from deep-level centers can create nontrivial and non-

Downloaded 11 Mar 2010 to 131.155.151.137. Redistribution subject to AIP license or copyright; see http://jap.aip.org/jap/copyright.jsp

stationary profile of initial carriers in the n base. However, our theory reveals weak logarithmic dependence of all major front parameters on n_0 and p_0. This justifies our assumption that n_0 and p_0 maintain constant values in the depleted region.
[27] *Handbook Series on Semiconductor Parameters*, edited by M. E. Levinstein, S. L. Rumyntsev, and M. S. Shur (World Scientific, London, 1996), Vol. 1.
[28] C. Jacoboni, C. Canali, G. Ottaviani, and A. Alberigi, Solid-State Electron. **20**, 77 (1977).
[29] S. M. Sze, *Physics of Semiconductor Devices* (Wiley, New York, 1981).
[30] E. M. Bazelyan and Yu. P. Raizer, *Spark Discharges* (CRC Press, New York, 1998).
[31] M. I. D'yakonov and V. Yu. Kachorovskii, Sov. Phys. JETP **67**, 1049 (1988) [Zh. Eksp. Teor. Fiz. **94**, 321 (1988)].
[32] M. I. D'yakonov and V. Yu. Kachorovskii, Sov. Phys. JETP **68**, 1070 (1989) [Zh. Eksp. Teor. Fiz. **95**, 1850 (1989)].

Downloaded 11 Mar 2010 to 131.155.151.137. Redistribution subject to AIP license or copyright; see http://jap.aip.org/jap/copyright.jsp